Coherent population transfer with polariton states in circuit QED

Madan Mohan Mahana,[1] Sankar Davuluri,[2] and Tarak Nath Dey [1,*]

[1]*Department of Physics, Indian Institute of Technology Guwahati, Guwahati 781039, Assam, India*
[2]*Department of Physics, Birla Institute of Technology and Science Pilani, Hyderabad Campus, Hyderabad 500078, India*

The stimulated Raman adiabatic passage (STIRAP) allows selective, coherent population transfer in a three-level quantum system by the adiabatic control of two suitably chosen envelopes and delayed laser pulses. However, the long operation time involved with the adiabatic protocols makes them more susceptible to decay and decoherence. A shortcut-to-adiabaticity technique, namely, counterdiabatic driving (CD), suppresses the decoherence-induced loss by speeding up the STIRAP process, thereby enhancing the efficiency and fidelity of population transfer. The superadiabatic STIRAP (saSTIRAP) method requires the application of a shortcut drive or CD pulse, which couples the coherently trapped states in a three-level quantum system. Hence, the closed-loop Λ system consisting of all electric dipole-allowed transitions is an essential requirement for saSTIRAP, which is rarely admissible in a natural atom. This paper theoretically investigates an experimentally feasible model for implementing saSTIRAP using a closed-loop Λ system with doubly dressed polariton states in a driven circuit QED system. We show a population transfer with efficiencies close to 80.75% and 98.10% with fidelities of 89.86% and 99.04% for the resonant STIRAP and saSTIRAP protocols, respectively, with experimentally feasible parameters. The efficiency of the population transfer can be further increased by improving the coherence times of the cavity and the transmon qubit. This work may be useful in designing fast, efficient quantum gates for applications in quantum technologies.

I. INTRODUCTION

Precise manipulation and control of the quantum states in a system are an essential task for efficient quantum technologies [1,2]. The stimulated Raman adiabatic passage (STIRAP) is a robust, powerful adiabatic protocol in quantum optics for selective, faithful coherent population transfer, entangled-state preparation, etc. [3]. This protocol is robust against the fluctuations in experimental parameters due to slow adiabatic control of quantum states over long operation times. The shortcut-to-adiabaticity (STA) techniques developed in the last decade reduce the operation time of adiabatic protocols, thereby minimizing decoherence-induced losses and improving the efficiency [4]. An STA technique, namely, counterdiabatic driving (CD) drive, can speed up the STIRAP protocol and enhance the fidelity of population transfer to achieve superadiabatic STIRAP (saSTIRAP) [5,6]. Recent advancements in solid-state quantum devices like superconducting quantum circuits (SQCs) have led to growing interest in studying multilevel coherent phenomena in quantum optics in the microwave regime [7]. The on-chip tunability, rapid improvement in the coherence time of superconducting artificial atoms or qubits (SAAs), and scalability make the SQCs a versatile solid-state platform for quantum technologies and microwave quantum optics [8]. However, the implementation of the STIRAP and saSTIRAP protocols in SQCs is still largely unexplored.

In quantum optics, counterintuitive phenomena such as electromagnetically induced transparency (EIT) [9], Autler-Townes splitting (ATS) [10], and coherent population trapping (CPT) [11] have a significant role in the precise control of the optical property of a medium. These atomic coherence-based experiments demand an atomic configuration with a larger atomic coherence lifetime. A three-level Λ system containing two longer-lived lower-level metastable states fulfills said criterion. Hence, three-level Λ systems with large anharmonicity and fewer decaying states are more suitable for realizing these quantum optical phenomena. Three-level quantum systems in SQCs have been used to demonstrate EIT [12,13], ATS [14–16], and CPT [17].

STIRAP is another prominent counterintuitive phenomenon in which robust population transfer between two nondegenerate metastable levels is possible without loss of generality [18]. In STIRAP, a suitable choice of two time-dependent coherent pulses coupled to two arms of a three-level Λ system allows a complete population transfer from the ground state to the target metastable state without populating the intermediate excited state. In the last few decades, many theoretical studies have been devoted to the implementation of STIRAP systems with SQCs [19–24]. STIRAP has been experimentally realized in many quantum optical systems, including SQCs [25,26]. Adiabatic protocols like STIRAP are associated with a slow change in controls, which leaves some dynamic properties invariant. In the quantum regime, slow processes with long operation times are badly affected by decoherence, which produces unwanted losses and perturbations. STA methods are well-established techniques to speed up the adiabatic protocols and achieve the same final results while bypassing the strict adiabatic conditions [27]. CD [28], the Lewis-Riesenfeld

---

023716-1

invariant method [29,30], and the dressed-state approach [31] are among the STA techniques [32] readily used to speed up the adiabatic quantum protocols. Very recently, a CD protocol with STIRAP was successfully implemented in a three-level ladder-type superconducting transmon qutrit [6]. The superadiabatic population transfer (saSTIRAP) from the ground state to the qutrit's second excited state was achieved using a two-photon CD pulse driving the transition between these states. However, two-photon detuning producing small ac Stark shifts to all the energy levels is a drawback of the system. This issue could be resolved by a complex process of dynamically modifying the phases of all the applied drives, thus leaving the scope for a better scheme for the demonstration of saSTIRAP in SQCs. Applying the CD pulse to a Λ system requires driving the transition from the initial ground state to the target metastable state, forming a closed-loop Λ system. Therefore, the possibility of implementing saSTIRAP using a closed-loop Λ system in SQCs is worth exploring. To the best of our knowledge, there has not been a theoretical investigation of saSTIRAP with a closed-loop Λ system in SQCs yet.

The experimental realization of Λ systems with metastable states in SQCs has been elusive. The implementation of a dressed-state-engineered impedance-matched Λ system in the doubly dressed polariton basis was investigated in Ref. [33]. It opened up avenues for theoretical and experimental demonstration of several quantum optical applications with Λ systems in SQCs [34–36]. The implementation of EIT with an identical system was theoretically proposed in Ref. [37] and was experimentally realized with the polariton states generated with a rf-biased transmon qubit coupled to a resonator [38]. With all the dipole-allowed transitions, a closed-loop Λ configuration is possible in this system, which is impossible in natural atoms. We exploit this advantage to theoretically investigate the implementation of the STIRAP and saSTIRAP protocols with a driven circuit QED system. We use the doubly dressed polariton states instead of the qutrit states [6] used recently to study the coherent transfer of population in SQCs. The SAAs, such as flux qubits [20], are operated away from the sweet spots to break the parity-selection rule and form closed-loop Λ-type configurations. All transitions in such SAAs are allowed away from the sweet spots at the cost of lower coherence lifetimes [39]. However, the driven circuit QED system suggested in this paper remedies this issue while maintaining the sweet spot's coherence properties.

The rest of this paper is organized as follows. In Sec. II, we describe the theoretical model of the Hamiltonian and the tunable transition rates of a Λ system in a driven circuit QED system. We discuss the theoretical proposal for implementing the CD protocol for saSTIRAP with a closed-loop Λ system in Sec. III. Section IV thoroughly discusses the significant numerical results. Finally, we conclude our investigation in Sec. V.

II. THEORETICAL MODEL

This section deliberates the theoretical model for realizing a Λ system in circuit QED. First, we describe the Hamiltonian of the model, then derive the expression for transition rates of the Λ system.
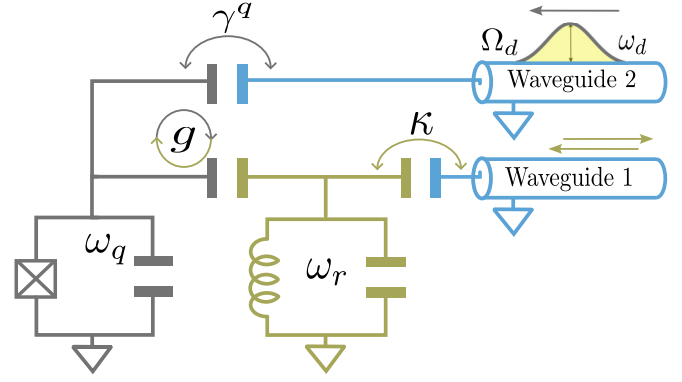

FIG. 1. A schematic lumped-element circuit diagram of a driven circuit QED system. Here, a classical microwave field with coupling strength Ω_d drives a transmon (gray) with frequency ω_d, further capacitively coupled to a single-mode cavity (green) with coupling strength g. The transmon and cavity are capacitively coupled to two independent semi-infinite waveguides (blue).

A. Model Hamiltonian

The ability to precisely control a quantum system's population at various levels is challenging due to decay-induced population loss. The STIRAP is an indispensable tool for transferring the population to the desired levels and overcoming decay-induced population losses. A counterintuitive pair of laser pulses is used in the STIRAP. A pump pulse couples an initial populated ground state with an excited state, whereas an advanced Stokes pulse couples an unoccupied metastable state and an excited state. The two lower-level metastable states coupling with the intermediate excited state by the coherent pulses form a Λ-type configuration. In this level geometry, the efficiency and robustness of the population transfer are sensitive to the overlaps between the Stokes and pump fields and the individual pulse area. The slow rate of population transfer in STIRAP is the obstacle to efficient population transfer and the reason behind the population loss. Hence, faster population-transfer processes such as saSTIRAP can avoid inherent decay and decoherence limitations. This work explores speeding up STIRAP passage in circuit quantum electrodynamics by considering a closed-looped Λ system in which the ground and metastable states can be directly coupled. The scheme for a coupled transmon-cavity system is shown schematically in Fig. 1. The cavity and the transmon are connected to semi-infinite waveguides 1 and 2, respectively. Through waveguide 2, a microwave field with coupling strength Ω_d drives a two-level transmon with frequency ω_d, further capacitively coupled to a single-mode cavity with coupling strength g. The total Hamiltonian of the system can be cast as follows:

$$\hat{H}_0 = \frac{\hbar}{2}\omega_q\hat{\sigma}_z + \hbar\omega_r\left(\hat{a}^\dagger\hat{a} + \frac{1}{2}\right) + \hbar g(\hat{a}^\dagger\hat{\sigma}_- + \hat{a}\hat{\sigma}_+)$$
$$+ \hbar\Omega_d\left(\hat{\sigma}_-e^{i\omega_d t} + \hat{\sigma}_+e^{-i\omega_d t}\right), \tag{1}$$

where ω_q and ω_r stand for the transmon and cavity frequencies, respectively. The transmon is basically a weakly anharmonic oscillator. However, the transmon can be effectively treated as a two-level system by the suppression of excitation

to higher noncomputational states using robust control techniques such as a derivative-reduction-by-adiabatic-gate pulse [40]. Here, we use a two-level transmon for the simplicity of the calculations, as used in recent works [13,38]. The annihilation and creation operators of the cavity are denoted by $\hat{a}$ and $\hat{a}^\dagger$, and the atomic lowering and raising operators for the transmon are $\hat{\sigma}_-$ and $\hat{\sigma}_+$. The interaction strength and frequency of the classical microwave field are expressed by the parameters Ω_d and ω_d, respectively. We eliminate the explicit time-dependent factors of the Hamiltonian by transforming the Hamiltonian into a rotating frame using a unitary operator $U = e^{-i\omega_d t(\hat{\sigma}_z/2 + \hat{a}^\dagger \hat{a})}$ and obtain the effective Hamiltonian

$$
\hat{H}_{\text{RWA}} = \frac{\hbar}{2}\tilde{\omega}_q \hat{\sigma}_z + \hbar\tilde{\omega}_r\left(\hat{a}^\dagger\hat{a} + \frac{1}{2}\right) + \hbar g(\hat{a}^\dagger\hat{\sigma}_- + \hat{a}\hat{\sigma}_+) \\
+ \hbar\Omega_d[\hat{\sigma}_- + \hat{\sigma}_+] \tag{2}
$$

under the rotating-wave approximation. Here, $\tilde{\omega}_q = \omega_q - \omega_d$, $\tilde{\omega}_r = \omega_r - \omega_d$, and $\tilde{\Delta} = \tilde{\omega}_r - \tilde{\omega}_q$ is the cavity-transmon detuning. The first three terms in the Hamiltonian can be identified as the celebrated Jaynes-Cummings model. The last term represents the interaction between the external classical microwave drive field and the two-level transmon. The eigenstates of the Jaynes-Cummings Hamiltonian are known as the dressed states, which can be denoted as

$$
|+, n\rangle = \cos\frac{\theta_n}{2}|e, n\rangle + \sin\frac{\theta_n}{2}|g, n+1\rangle, \tag{3}
$$

$$
|-, n\rangle = -\sin\frac{\theta_n}{2}|e, n\rangle + \cos\frac{\theta_n}{2}|g, n+1\rangle, \tag{4}
$$

where $\tan\theta_n = -2g\sqrt{n+1}/\tilde{\Delta}$. Here, $|e, n\rangle$ and $|g, n\rangle$ denote that the qubit is in the excited state $|e\rangle$ and ground state $|g\rangle$, respectively, whereas the single-mode cavity is in state $|n\rangle$. The corresponding eigenenergies of the dressed states are

$$
E_{\pm, n} = \hbar\tilde{\omega}_r(n+1) \pm \frac{\hbar}{2}\sqrt{\tilde{\Delta}^2 + 4g^2(n+1)}. \tag{5}
$$

Further mixing of these dressed states in the dispersive regime ($g \ll \tilde{\Delta}$) by the external microwave field applied to drive the transmon gives doubly dressed polariton states. Polaritons are referred to as quasiparticles carrying elementary excitations of the light-matter interaction. These polariton states can be denoted by $|i\rangle$ and $|j\rangle$, with the corresponding eigenenergies ω_i and ω_j ($i, j = 1, 2, 3, 4, \dots$). The polariton states can be engineered to obtain a nested four-level system consisting of the lowest four eigenstates of (2) by restricting the driving field to satisfy the condition $\omega_q - 3\chi < \omega_d < \omega_q - \chi$, where $\chi = g^2/\tilde{\Delta}$ denotes the dispersive frequency shift ([33,37]; also see Appendix B). Under the so-called nesting regime, levels $|1\rangle$, $|3\rangle$ (or $|4\rangle$), and $|2\rangle$ form a Λ system configuration, as shown in Fig. 2. We denote states $|1\rangle$, $|2\rangle$, and $|3\rangle$ as the ground state, metastable state, and excited state, respectively.

B. Transition rates

Waveguides 1 and 2 are coupled to the cavity and transmon to apply drive and readout signals. We consider two waveguides as external environments, and the total Hamiltonian of the open quantum system can be written as

$$
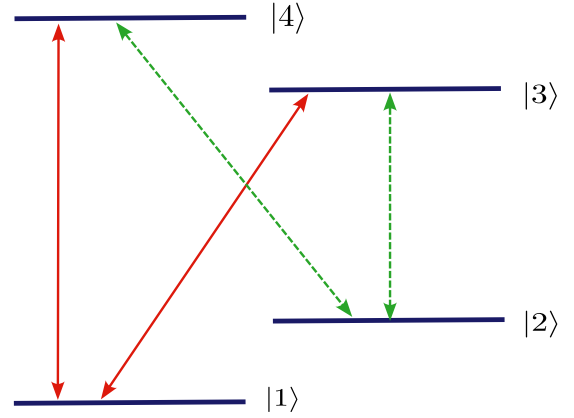\hat{H}_T = \hat{H}_S + \hat{H}_E + \hat{H}_I, \tag{6}
$$

FIG. 2. Energy-level diagram of the doubly dressed polariton states in the driven circuit QED system. The solid red and dashed green arrows represent the two arms of the Λ system constructed by using the states $|1\rangle$, $|3\rangle$ (or $|4\rangle$), and $|2\rangle$ in the doubly dressed polariton basis.

where $\hat{H}_S$, $\hat{H}_E$, and $\hat{H}_I$ denote the Hamiltonians of the system, the environment, and the system-environment interaction, respectively. We consider Eq. (1) to be the Hamiltonian of the system $\hat{H}_S$. The Hamiltonian of the environment $\hat{H}_E$ is expressed as

$$
\hat{H}_E = \hbar\int\omega\hat{b}^\dagger(\omega)\hat{b}(\omega)d\omega + \hbar\int\omega'\hat{c}^\dagger(\omega')\hat{c}(\omega')d\omega', \tag{7}
$$

where $\hat{b}$ and $\hat{c}$ denote the annihilation operators in waveguide 1 and waveguide 2, respectively, and $\hat{b}^\dagger$ and $\hat{c}^\dagger$ represent the corresponding creation operators. The system-environment interaction Hamiltonian is denoted by $\hat{H}_I$ and can be defined as

$$
\hat{H}_I = \hbar\left[\int d\omega K(\omega)\hat{b}^\dagger(\omega)\hat{a} + \text{H.c.}\right] \\
+ \hbar\left[\int d\omega'\eta(\omega')\hat{c}^\dagger(\omega')\hat{\sigma}_- + \text{H.c.}\right]. \tag{8}
$$

The Hamiltonians $\hat{H}_E$ and $\hat{H}_I$ remain unchanged in the rotating frame. For simplicity, we can consider having flat spectra in the environments, so that both coupling strengths $K(\omega)$ and $\eta(\omega')$ can be considered constants. Thus, by introducing the first Markov approximation, we can get

$$
K(\omega) = \sqrt{\frac{\kappa}{2\pi}}, \tag{9}
$$

$$
\eta(\omega') = \sqrt{\frac{\gamma^q}{2\pi}}, \tag{10}
$$

where κ and γ^q denote the decay rates of the cavity and the transmon into waveguides 1 and 2, respectively. For simplicity, the inherent (nonradiative) decay rates of the transmon qubit and the cavity are included in γ^q and κ, respectively [34]. Let us write the operators $\hat{a}$ and $\hat{\sigma}_-$ in the polariton basis:

$$
\hat{a} = \sum_{ij}\langle i|\hat{a}|j\rangle\hat{\sigma}_{ij}, \tag{11}
$$

$$
\hat{\sigma}_- = \sum_{ij}\langle i|\hat{\sigma}_-|j\rangle\hat{\sigma}_{ij}, \tag{12}
$$

Parameter	Value	Parameter	Value (2π MHz)
C_{31}	0.77	ω_{31}	5101
C_{32}	0.64	ω_{32}	5023
C_{21}	0.08	ω_{21}	78
Q_{31}	0.00	γ_{31}	1.78
Q_{32}	0.10	γ_{32}	1.23
Q_{21}	0.82	γ_{21}	0.05

where $|i\rangle$ and $|j\rangle$ denote the polariton states and $\hat{\sigma}_{ij} = |i\rangle\langle j|$. In the polariton basis, the Hamiltonian H_I can be recast into the following form:

$$\hat{H}_I = \hbar \int d\omega \sum_{ij} \left[\sqrt{\frac{\kappa_{ij}}{2\pi}} \hat{b}^\dagger(\omega)\hat{\sigma}_{ij} + \text{H.c.} \right]$$
$$+ \hbar \int d\omega' \sum_{ij} \left[\sqrt{\frac{\gamma^q_{ij}}{2\pi}} \hat{c}^\dagger(\omega')\hat{\sigma}_{ij} + \text{H.c.} \right], \quad (13)$$

where κ_{ij} and γ^q_{ij} are the radiative decay rates into waveguide 1 and waveguide 2, respectively, for the transition from polariton state $|i\rangle$ to $|j\rangle$. The transition rates κ_{ij}, γ^q_{ij} are defined as

$$\kappa_{ij} = \kappa |\langle i|\hat{a}^\dagger|j\rangle|^2, \quad (14)$$

$$\gamma^q_{ij} = \gamma^q |\langle i|\hat{\sigma}_+|j\rangle|^2. \quad (15)$$

Hence, we can determine the total radiative decay rate γ_{ij} for the transition between polariton states $|i\rangle$ and $|j\rangle$ as follows:

$$\gamma_{ij} = \kappa_{ij} + \gamma^q_{ij} = \kappa C^2_{ij} + \gamma^q Q^2_{ij}, \quad (16)$$

where the parameters $C_{ij} = |\langle i|\hat{a}^\dagger|j\rangle|$ and $Q_{ij} = |\langle i|\hat{\sigma}_+|j\rangle|$ represent the transition matrix elements corresponding to external drives applied to the cavity and the qubit, respectively. The energies of the polariton states can be tuned by the frequency ω_d and the Rabi frequency Ω_d of the classical microwave drive field applied to the transmon through waveguide 2. Thus, the decay rates γ_{ij} can also be tuned by varying the above parameters. One can design a Λ system with fixed energy levels and transition rates by assigning constant values to these parameters. The list of numerically computed values of the relevant parameters for our Λ system is given in Table I. We have used the experimentally feasible parameters [13,37] in the numerical simulations for our model system.

III. COUNTERDIABATIC DRIVING

The STIRAP process can be implemented with the three-level Λ system described in Sec. II. The matrix representation of the STIRAP Hamiltonian under the rotating-wave

approximation is

$$\hat{H}(t) = \frac{\hbar}{2} \begin{pmatrix} 0 & \Omega_p(t) & 0 \\ \Omega_p(t) & 2\Delta & \Omega_s(t) \\ 0 & \Omega_s(t) & 2\delta \end{pmatrix}, \quad (17)$$

where $\Omega_p(t)$ and $\Omega_s(t)$ denote the coupling strengths of the time-dependent pump and Stokes fields for driving the $|3\rangle \leftrightarrow |1\rangle$ and $|3\rangle \leftrightarrow |2\rangle$ transitions with frequencies ω_p and ω_s, respectively. The parameters Δ and δ denote the one-photon detuning $\Delta = (\omega_{31} - \omega_p)$ and two-photon detuning $\delta = (\omega_{31} - \omega_p) - (\omega_{32} - \omega_s)$, respectively. Here, the energy levels of the Λ system satisfy $E_1 < E_2 < E_3$. The one-photon detuning Δ differs from the cavity-transmon detuning $\tilde{\Delta}$, discussed in the last section. For a perfectly resonant STIRAP process, i.e., $\Delta = \delta = 0$, the instantaneous eigenvalues of the above Hamiltonian are $E_0 = 0$ and $E_\pm = \pm\hbar\Omega_0(t)/2$, with $\Omega_0(t) = \sqrt{\Omega_p^2(t) + \Omega_s^2(t)}$. The corresponding instantaneous eigenstates are given by

$$|n_0(t)\rangle = \begin{pmatrix} \cos\theta(t) \\ 0 \\ -\sin\theta(t) \end{pmatrix}, \quad |n_\pm(t)\rangle = \frac{1}{\sqrt{2}} \begin{pmatrix} \sin\theta(t) \\ \pm 1 \\ \cos\theta(t) \end{pmatrix}, \quad (18)$$

where $\tan\theta(t) = \Omega_p(t)/\Omega_s(t)$. Perfect adiabatic population transfer from state $|1\rangle$ to $|2\rangle$ can be achieved by following the dark state $|n_0(t)\rangle$ under the local adiabatic condition $|\dot{\theta}| \ll |\Omega_0|$ that needs to be fulfilled [41].

To speed up the STIRAP protocol, one can apply an additional coupling field driving the $|2\rangle \leftrightarrow |1\rangle$ transition [5,28,42]. The additional drive is termed a counterdiabatic drive or transitionless quantum drive, and it can be expressed as

$$\hat{H}^{\text{CD}}(t) = i\hbar \sum_n [|\partial_t n(t)\rangle\langle n(t)| - \langle n(t)|\partial_t n(t)\rangle|n(t)\rangle\langle n(t)|]. \quad (19)$$

We derive the Hamiltonian $\hat{H}^{\text{CD}}(t)$ using the adiabatic basis states $|n(t)\rangle = (|n_0(t)\rangle, |n_\pm(t)\rangle)$, which reads

$$\hat{H}^{\text{CD}}(t) = \frac{\hbar}{2} \begin{pmatrix} 0 & 0 & i\Omega_a(t) \\ 0 & 0 & 0 \\ -i\Omega_a(t) & 0 & 0 \end{pmatrix}, \quad (20)$$

where $\Omega_a(t) = 2\dot{\theta}(t)$ and the overdot denotes the first derivative with respect to time. We assume that the external drives are applied to the dressed-state-engineered Λ system with polariton states by driving the cavity and the transmon qubit. The Hamiltonian representing the interaction between the cavity, transmon, and external drive fields is thus given by

$$\hat{H}_d = \frac{\hbar}{2}(A_p\hat{a}^\dagger e^{-i\omega_p t} + A_s\hat{a}^\dagger e^{-i\omega_s t} + A_a\hat{\sigma}_+ e^{-i\omega_a t} + \text{H.c.}), \quad (21)$$

where the pump field and Stokes field with frequencies ω_p and ω_s, respectively, are coupled to the cavity through waveguide 1, with coupling strengths A_p and A_s. The additional drive field, i.e., counterdiabatic drive with frequency ω_a, is coupled to the transmon qubit through waveguide 2, with coupling strength A_a. Considering the pump field, Stokes field, and counterdiabatic drive field are driving the $|3\rangle \leftrightarrow |1\rangle$, $|3\rangle \leftrightarrow |2\rangle$, and $|2\rangle \leftrightarrow |1\rangle$ transitions in the polariton basis, respectively, we define the amplitudes of the respective Rabi frequencies of the external drive fields in the polariton basis
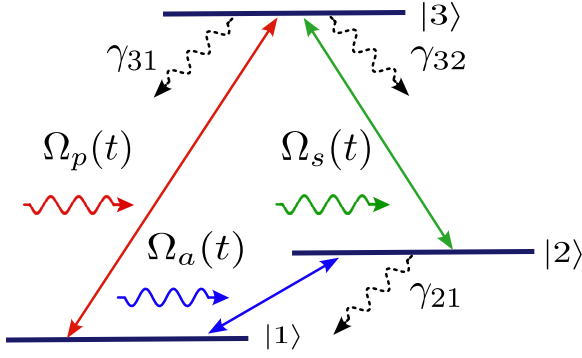
FIG. 3. The schematic diagram of a three-level closed-loop Λ system driven by three external classical fields, $\Omega_p(t)$, $\Omega_s(t)$, and $\Omega_a(t)$, driving the $|3\rangle \leftrightarrow |1\rangle$, $|3\rangle \leftrightarrow |2\rangle$, and $|2\rangle \leftrightarrow |1\rangle$ transitions, respectively.

as

$$\Omega_p \approx A_p C_{31}, \quad \Omega_s \approx A_s C_{32}, \quad \Omega_a \approx A_a Q_{21}, \quad (22)$$

where the parameters C_{31}, C_{32}, and Q_{21} are the transition matrix elements already defined in Sec. II. Here, Ω_p, Ω_s, and Ω_a denote the peak Rabi frequencies of the external drives coupled to the closed-loop Λ system in the polariton basis, as shown in Fig. 3. Here, the Gaussian envelopes of the pump and Stokes fields are considered and stated as

$$\Omega_p(t) = \Omega_p e^{-\frac{t^2}{2\sigma^2}}, \quad (23)$$

$$\Omega_s(t) = \Omega_s e^{-\frac{(t-t_s)^2}{2\sigma^2}}. \quad (24)$$

Using Eqs. (17)–(20), one can obtain

$$\Omega_a(t) = -\frac{t_s}{\sigma^2} \operatorname{sech}\left[-\frac{t_s}{\sigma^2}\left(t - \frac{t_s}{2}\right)\right], \quad (25)$$

with the assumption of $\Omega_p = \Omega_s$ for brevity. Equation (25) shows that the counterdiabatic drive should have a Rabi frequency $\Omega_a = -t_s/\sigma^2$ with a sec-hyperbolic shape for the given pump and Stokes fields. Assuming that the intrinsic phases of the pump field, the Stokes field, and the CD drive field are ϕ_p, ϕ_s, and ϕ_a, respectively, we can write the total Hamiltonian of the system under the rotating-wave approximation as

$$\hat{\tilde{H}}(t) = \frac{\hbar}{2}[\Omega_p(t)|3\rangle\langle 1| + \Omega_s(t)|3\rangle\langle 2| - i\Omega_a(t)|2\rangle\langle 1| + \text{H.c.}], \quad (26)$$

where the relative phase of the closed-loop Λ system is $-\pi/2$ (i.e., $\phi = \phi_a + \phi_s - \phi_p = -\pi/2$ or $e^{i\phi} = -i$) as per Eq. (20) under the resonant driving conditions ($\delta = \Delta = 0$), $\omega_p = \omega_{31}$, $\omega_s = \omega_{32}$, and $\omega_a = \omega_{21}$. In order to solve the time evolution of the system, we adopt the Lindblad master equation [43,44]

$$\dot{\rho} = \frac{1}{i\hbar}[\hat{\tilde{H}}, \hat{\rho}] + \sum_{j=1}^{3} \mathcal{L}(\hat{\mathcal{O}}_j)\hat{\rho}, \quad (27)$$

where $\mathcal{L}(\hat{\mathcal{O}}_j)\rho = (2\hat{\mathcal{O}}_j\hat{\rho}\hat{\mathcal{O}}_j^\dagger - \hat{\rho}\hat{\mathcal{O}}_j^\dagger\hat{\mathcal{O}}_j - \hat{\mathcal{O}}_j^\dagger\hat{\mathcal{O}}_j\hat{\rho})/2$ represents the Lindblad superoperator. Here, the operators $\hat{\mathcal{O}}_j$
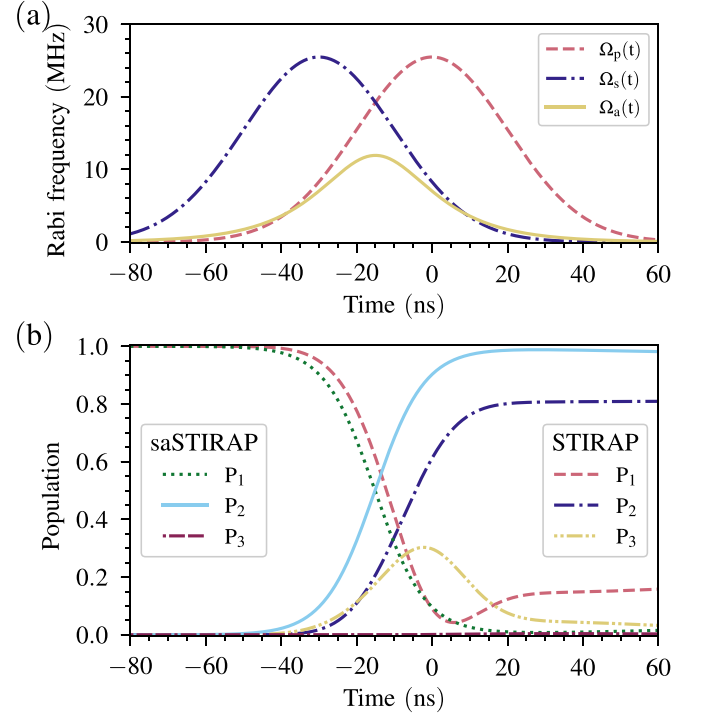

FIG. 4. (a) The pulse sequence of the three external classical drive fields, $\Omega_p(t)$, $\Omega_s(t)$, and $\Omega_a(t)$. (b) The time evolution of populations P_1, P_2, and P_3 during the STIRAP ($\Omega_a = 0$) and saSTRIAP protocols. The parameters used for the simulation are $\Omega_p/2\pi = 25.5$ MHz, $\Omega_s/2\pi = 25.5$ MHz, $t_s = -30$ ns, $\sigma = 20$ ns, and all the parameters given in Table I.

denote the jump operators given by $\hat{\mathcal{O}}_1 = \sqrt{\gamma_{31}}|1\rangle\langle 3|$, $\hat{\mathcal{O}}_2 = \sqrt{\gamma_{32}}|2\rangle\langle 3|$, and $\hat{\mathcal{O}}_3 = \sqrt{\gamma_{21}}|1\rangle\langle 2|$. We substitute the drive fields given in Eqs. (23)–(25) in Eq. (26) and numerically solve the time evolution of the system using the Lindblad master equation given in Eq. (27). The well-established mesolve routine in QUTIP [45,46] is used for solving the time-dependent Lindblad master equations. The numerical results are discussed in the following section.

IV. RESULTS AND DISCUSSION

We split this section into three parts describing the significant findings of this work. Section IV A highlights the dynamics of coherent population transfer in our system. The sensitivity of the coherent transfer protocols to variations in the parameters is discussed in Sec. IV B. We quantitatively compare the efficiencies of coherent population-transfer protocols by numerically computing the fidelity in Sec. IV C.

A. Coherent population transfer

We investigate the population dynamics in each energy level of the Λ system described in Sec. III. Figure 4(a) shows the pulse sequence of three external drive fields applied to the polariton-state-Λ system by driving the cavity mode or the transmon qubit. The Lindblad master equations for the STIRAP and saSTIRAP protocols for the Λ system are numerically solved by using the Hamiltonian (26) to study
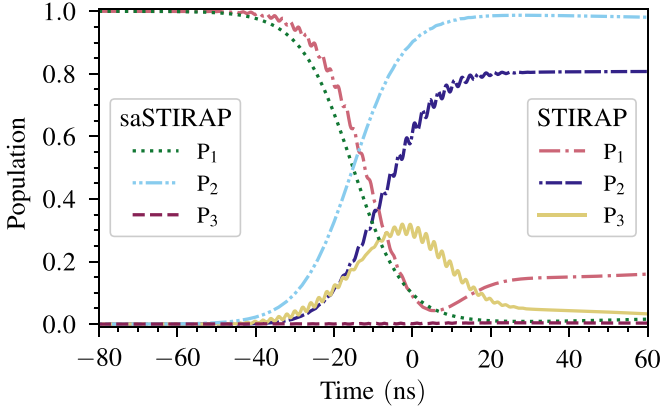
FIG. 5. The time evolution of populations P_1, P_2, and P_3 during the STIRAP ($\Omega_a = 0$) and saSTIRAP protocols with cross talk between the $|3\rangle \leftrightarrow |1\rangle$ and $|3\rangle \leftrightarrow |2\rangle$ transitions. The parameters used for the simulation are $\Omega_p/2\pi = 25.5$ MHz, $\Omega_s/2\pi = 25.5$ MHz, $t_s = -30$ ns, $\sigma = 20$ ns, and all the parameters given in Table I.

the population dynamics. A counterdiabatic drive is applied to the Λ system to realize the saSTIRAP by coupling the $|2\rangle \leftrightarrow |1\rangle$ transition, as mentioned in the last section. Figure 4(b) substantiates that one can achieve faster coherent population transfer from level $|1\rangle$ to $|2\rangle$ by applying the CD protocol compared to the STIRAP in the Λ system in the polariton basis. The populations P_1, P_2, and P_3 denote the populations in polariton states $|1\rangle$, $|2\rangle$, and $|3\rangle$, which are simply the density-matrix elements $\hat{\rho}_{11}$, $\hat{\rho}_{22}$, and $\hat{\rho}_{33}$, respectively, in the polariton basis.

The numerical results indicate that 80.92% of the population can be transferred from the ground state to the metastable state by the STIRAP protocol with experimentally feasible parameters for our model system [13,37]. However, one can achieve a much higher efficiency of 98.16% population transfer with the saSTIRAP protocol with the same parameters. There is a possibility of cross talk among the $|3\rangle \leftrightarrow |1\rangle$ and $|3\rangle \leftrightarrow |2\rangle$ transitions in the presence of applied pump and Stokes fields which resonantly couple the $|3\rangle \leftrightarrow |1\rangle$ and $|3\rangle \leftrightarrow |2\rangle$ transitions, respectively. The transition frequency of the $|3\rangle \leftrightarrow |1\rangle$ transition is close to that of the $|3\rangle \leftrightarrow |2\rangle$ transition that leads to the cross talk. In that case, the interaction Hamiltonian (26) can be rewritten as

$$\hat{\tilde{H}}'(t) = \hat{\tilde{H}} + \frac{\hbar}{2}[\Omega_p(t)e^{i(\omega_s - \omega_p)t}|3\rangle\langle 2|$$
$$+ \Omega_s(t)e^{i(\omega_p - \omega_s)t}|3\rangle\langle 1| + \text{H.c.}]. \quad (28)$$

The cross-driving terms may seem to alter the energy levels of the three-level system by inducing intensity-dependent Stark shifts, thereby impacting the efficiency of the coherent population transfer. However, the Stark shifts in the energy levels induced by the cross-driving terms are very small ($\sim 10^{-5}$) in magnitude compared to the unperturbed energies of the polariton states and can be neglected as the peak Rabi frequencies Ω_p and Ω_s are very small compared to ω_{3j}, where $j = 1, 2$. The time evolution of the populations and the efficiency of coherent population transfer in the presence of the cross-driving terms are depicted in Fig. 5. There are noticeable small oscillations in the populations (predominantly for STIRAP). The
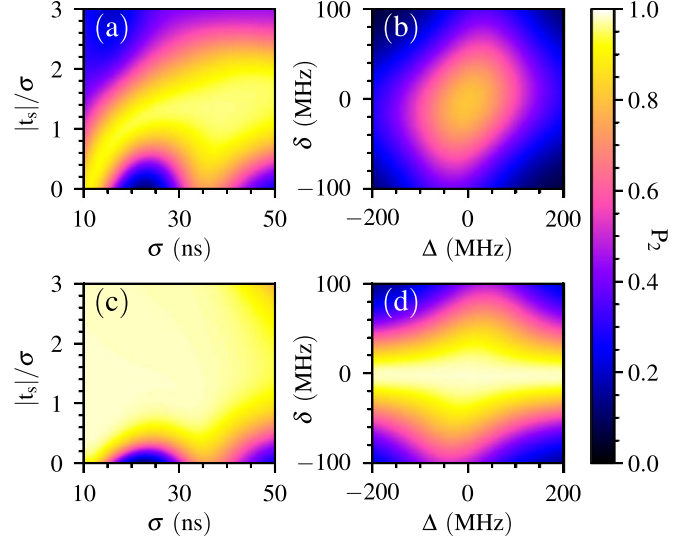

FIG. 6. The efficiency of the STIRAP (top) and saSTIRAP (bottom) protocols in the parameter space of (a) and (c) the pulse width σ and the normalized pulse separation $|t_s|/\sigma$ and (b) and (d) the one-photon detuning Δ and the two-photon detuning δ. The parameters used for the numerical simulation are $t_s = -30$ ns, $\sigma = 20$ ns, and the parameters used in Fig. 4.

numerical simulation of the Lindblad master equation with the Hamiltonian (28) suggests that we can achieve 80.75% (98.10%) population-transfer efficiency for the STIRAP (saSTIRAP) protocol, even in the presence of the cross-driving terms in the Hamiltonian (with $\omega_p - \omega_s = \omega_{21}$). Therefore, the cross talk among the $|3\rangle \leftrightarrow |1\rangle$ and $|3\rangle \leftrightarrow |2\rangle$ transitions in our closed-loop Λ system is not significantly detrimental to the efficiency of the coherent population transfer. Moreover, the efficiency of these protocols is also dependent on other important parameters, such as the pulse amplitudes and the pulse widths of the external drive fields, normalized pulse separation, etc., that we elaborate on in the following section.

B. Sensitivity to parameters

This section benchmarks the efficiency of the STIRAP and saSTIRAP protocols with the variation in the parameters used for numerical analysis. At the end of these protocols, we quantify the population-transfer efficiency by the final population in state $|2\rangle$. All the simulations in the rest of the paper are performed by using the Hamiltonian (28) in the Lindblad master equation (27) to include the effect of cross driving on the efficiency of coherent population transfer. Figures 6(a) and 6(c) show how the efficiency varies in the parameter space of the pulse width σ and the normalized pulse separation $|t_s|/\sigma$ for the STIRAP and saSTIRAP protocols, respectively. The parameters $\sigma = 20$ ns and $t_s = -30$ ns for $\Omega_p/2\pi = \Omega_s/2\pi = 25.5$ MHz lie in the highly efficient bright yellow regions in both panels. Figure 6(b) shows that the resonant driving condition ($\Delta = \delta = 0$) is ideal for highly efficient coherent population transfer in the STIRAP protocol. The nonzero two-photon detuning δ and single-photon detuning Δ give rise to nonadiabatic excitations and are detrimental to the efficiency of population transfer [47]. Figure 6(d) shows
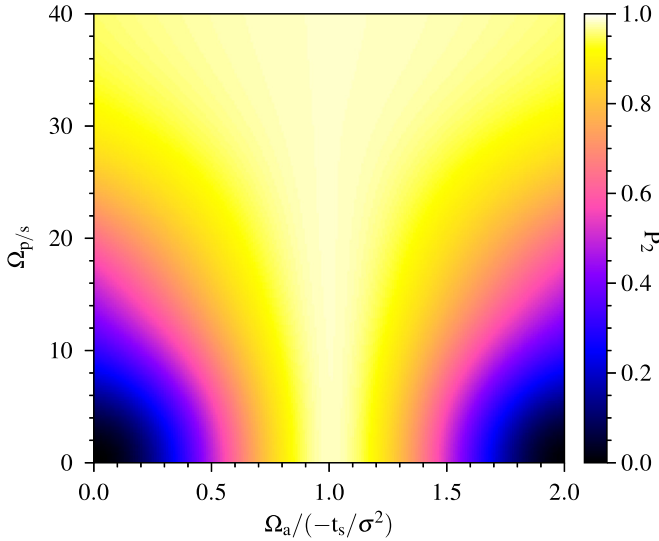
FIG. 7. Efficiency of the coherent population transfer with the saSTIRAP protocol in the parameter space of the peak Rabi frequencies of the pump and Stokes fields $\Omega_{p/s}$ (here, $\Omega_p = \Omega_s$) and the CD drive $\Omega_a/(-t_s/\sigma^2)$. The parameters used for the numerical simulation are $t_s = -30$ ns, $\sigma = 20$ ns, and the other parameters given in Table I.

the saSTIRAP protocol is more robust against one-photon detuning Δ than two-photon detuning δ. These plots further indicate that the saSTIRAP protocol is more efficient and robust than the STIRAP protocol for a closed-loop Λ system in circuit QED.

The variation in the efficiency of coherent population transfer in the parameter space of the peak Rabi frequencies of the pump and Stokes fields $\Omega_{p/s}$ and the CD drive (normalized with the numerical value of $-t_s/\sigma^2$) is illustrated in Fig. 7. We can observe that higher efficiency of coherent population transfer can be achieved with higher Rabi frequencies of the pump and Stokes fields. However, optimal efficiency can be achieved in the presence of a CD drive with a peak Rabi frequency $-t_s/\sigma^2$ even with the lower Rabi frequencies of the pump and Stokes fields.

C. Fidelity

In quantum information theory and quantum mechanics, the quantitative measure of the closeness of a quantum state at a final time t to the ideal target state is given by fidelity $\mathcal{F}$ [1] and is defined as

$$\mathcal{F}(\hat{\rho}_{\text{ideal}}, \hat{\rho}_t) = \text{Tr}\sqrt{\sqrt{\hat{\rho}_{\text{ideal}}}\,\hat{\rho}_t\,\sqrt{\hat{\rho}_{\text{ideal}}}}, \qquad (29)$$

where the density-matrix operators $\hat{\rho}_t$ and $\hat{\rho}_{\text{ideal}}$ describe the quantum state of the system at any time t and the ideal target state (here, $\hat{\rho}_{22}$). In Fig. 8(a), we show the time evolution of the fidelity between the quantum state of the system and the target state $|2\rangle$. One can observe that the fidelity of the saSTIRAP protocol is significantly higher than that of STIRAP over the operation time of the protocols.

Our numerical calculation suggests that the final fidelity for the saSTIRAP protocol is 99.04%, much higher than that of 89.86% for STIRAP, as shown by a dotted green curve and
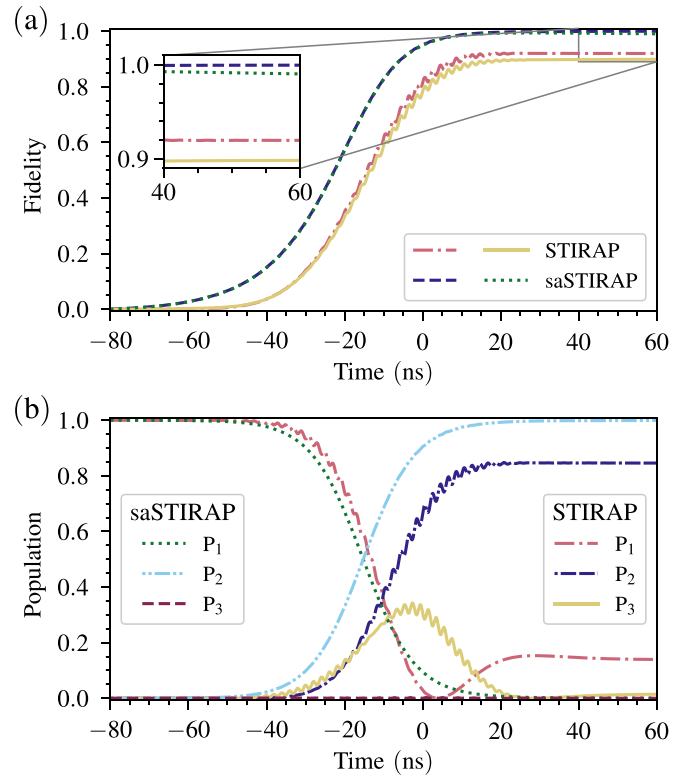

FIG. 8. (a) The fidelity of the STIRAP (saSTIRAP) protocol with radiative transitions is shown by the solid yellow (dotted green) line, and the dash-dotted red (dashed blue) line shows the fidelity with the radiative transition rates (γ_{21}, γ_{32}, and γ_{31}) set to zero. The inset depicts the final fidelities of population transfer for all the cases. (b) The time evolution of the populations in the STIRAP and saSTIRAP protocols with the radiative transition rates (γ_{21}, γ_{32}, and γ_{31}) set to zero. The numerical simulation uses all the parameters used in Fig. 6

a solid yellow curve in the inset of Fig. 8(a), respectively. The dash-dotted red and dashed blue lines in Fig. 8(a) show the fidelity of both protocols in the absence of the radiative transition rates, which is presented as an ideal scenario for achieving the maximum fidelity of population transfer. We can observe a significant increment in the fidelity for each protocol without the radiative decay of the polariton states, suggesting that higher fidelity can be achieved by reducing the decay rates of the cavity and the transmon qubit. Figure 8(b) shows the time evolution of the populations for each protocol without the radiative transitions, indicating higher efficiency of the population transfer. The wiggly pattern of the curves in both Figs. 8(a) and 8(b) can be attributed to the impact of cross-driving terms in the Hamiltonian (28). The numerical simulations suggest that 84.61% of the population can be transferred with 91.98% fidelity with the STIRAP protocol without the radiative decay of the polariton states. The saSTIRAP protocol can transfer 99.94% of the population with 99.97% fidelity with zero radiative transitions. Thus, we can realize more efficient, robust, and coherent population transfer by increasing the coherence time of the transmon qubit and superconducting microwave resonator, reducing the radiative transitions in the polariton basis.
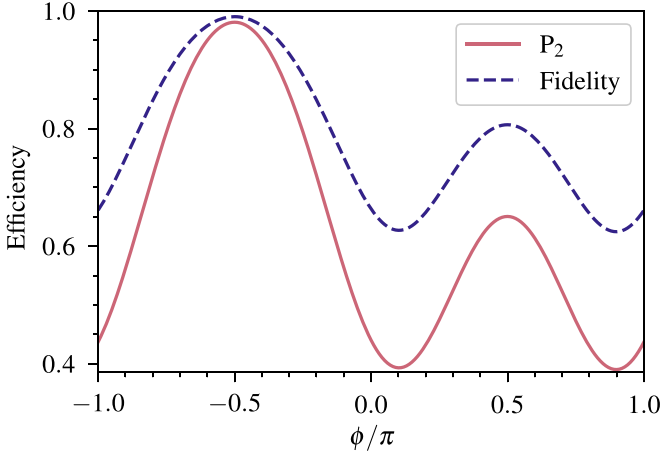
FIG. 9. The variation in the efficiency (final population P_2) and fidelity of coherent population transfer at the end of the saSTIRAP protocol with the variation in the relative phase ϕ of the closed-loop Λ system. The parameters used for the simulation are $\Omega_p/2\pi = 25.5$ MHz, $\Omega_s/2\pi = 25.5$ MHz, $t_s = -30$ ns, $\sigma = 20$ ns, and all the parameters given in Table I.

The variation in the final efficiency (solid red line) and fidelity (dashed blue line) shown in Fig. 9 substantiates that the relative phase in the closed-loop Λ system must be $-\pi/2$ as given in Eqs. (20) and (26) to achieve maximum efficiency of coherent population transfer through saSTIRAP. For simplicity, we consider that the inherent phases of the pump and Stokes fields are zero, and the CD drive has an inherent phase $-\pi/2$. One can achieve coherent population transfer with a maximum efficiency of 98.09% with 99.04% fidelity when $\phi = -\pi/2$ for the given parameters.

V. CONCLUSION

In conclusion, we theoretically investigated a physically conceivable model for implementing STIRAP and saSTIRAP in a driven circuit QED system. A circuit QED system resembles the famous Jaynes-Cummings model, which gives rise to hybridized cavity-qubit dressed states or polariton states. Further, these dressed states can be mixed with a strong microwave field driving the qubit, thereby forming doubly dressed polariton states. Thus, the driving field can tune the energy levels and decay rates of these polariton states. The dressed-state-engineered polariton states can allow a Λ or closed-loop Λ-type configuration under the so-called nesting regime of the drive field's frequency [33].

Our numerical analysis suggests that STIRAP- and saSTIRAP-assisted coherent population transfer in a closed-loop resonant Λ configuration is highly robust and efficient and may achieve efficiency comparable to or better than that of the current state-of-the-art coherent population-transfer protocols in SQCs [6,25,26]. The impact of cross driving was taken into account in the numerical simulations, which marginally reduces the efficiency ($\sim 0.06\%$) of the population transfer in our model system. The two-photon detuning, as well as large single-photon detuning, limits the efficiency of both the STIRAP and saSTIRAP methods due to nonadiabatic excitation-induced population losses that compromise

the robustness of the protocol [3]. Furthermore, we showed that the saSTIRAP protocol is more robust than the STIRAP protocol against the variation in other relevant parameters like pulse width σ, normalized pulse separation $|t_s|/\sigma$, and one-photon detuning Δ. The significant 17% enhancement of the efficiency of population transfer in saSTIRAP over the STIRAP technique supports this claim.

Our theoretical model can be realized experimentally with currently available on-chip fabrication technologies with SQCs. Furthermore, this work will pave the way for the implementation of modified versions of STIRAP, such as fractional STIRAP [48], frequency-modulated STIRAP [49], etc., and the sped-up versions (using STA techniques) of these protocols with Λ-type configurations in SQCs. The CD driving can also be used for fast preparation of the entangled states, such as the Schrödinger-cat states in circuit QED [50]. There have been many recent investigations for implementing robust, efficient geometric and holonomic quantum phase gates using the STA techniques in superconducting quantum circuits that may be prepared with Λ systems in circuit QED [51,52] for quantum computing and quantum information processing. One can also implement the other STA techniques to speed up the transfer protocol with such systems in circuit QED and compare the efficiency and fidelity.

APPENDIX A: THE DOUBLY DRESSED POLARITON STATES

Assuming that, initially, there is no external drive applied to the transmon qubit through waveguide 2 (i.e., $\Omega_d = 0$), the Hamiltonian (2) can be identified as a circuit QED system represented by the Jaynes-Cummings model. The Hilbert space of the circuit QED Hamiltonian is thus spanned by the states $|g, 0\rangle$ and the hybrid cavity-qubit states (dressed states) $|\pm, n\rangle$, as discussed in Sec. II A. The corresponding eigenenergies of the dressed states given by Eq. (5) can be further simplified as

$$
\begin{aligned}
E_{\pm,n} &= \hbar\tilde{\omega}_r(n+1) \pm \frac{\hbar}{2}\sqrt{\tilde{\Delta}^2 + 4g^2(n+1)} \\
&\simeq \hbar\tilde{\omega}_r(n+1) \pm \frac{\hbar\tilde{\Delta}}{2}\left(1 + \frac{2g^2(n+1)}{\tilde{\Delta}^2}\right) \\
&\simeq \hbar\tilde{\omega}_r(n+1) \pm \frac{\hbar\tilde{\Delta}}{2} \pm \frac{\hbar g^2(n+1)}{\tilde{\Delta}}.
\end{aligned} \tag{A1}
$$

In the large-detuning or dispersive regime (i.e., $\tilde{\Delta} \gg g$), these states can be approximately mapped to the product states (i.e., $|e, n\rangle, |g, n\rangle$). Therefore, it can be approximately assumed that $|g, 0\rangle \sim |g, 0\rangle, |-, 0\rangle \sim |e, 0\rangle, |+, 0\rangle \sim |g, 1\rangle, |-, 1\rangle \sim |e, 1\rangle, |+, 1\rangle \sim |g, 2\rangle$, and so on. The generalization of the above approximation for a few lower-level states can be expressed as $|-, n\rangle \sim |e, n\rangle$ and $|+, n\rangle \sim |g, n+1\rangle$. The expressions for the energies of these levels can be stated as

$$
\begin{aligned}
\omega_{g,n} &\approx \omega_{+,n-1} \\
&\approx E_{+,n-1}/\hbar \simeq n\tilde{\omega}_r + \tilde{\Delta}/2 + ng^2/\tilde{\Delta} \\
&\approx n(\tilde{\omega}_r + \chi) + \tilde{\Delta}/2
\end{aligned} \tag{A2}
$$

and

$$
\begin{aligned}
\omega_{e,n} &\approx \omega_{-,n} \\
&\approx E_{-,n}/\hbar \simeq (n+1)\tilde{\omega}_r - \tilde{\Delta}/2 - (n+1)g^2/\tilde{\Delta} \\
&\approx n(\tilde{\omega}_r - \chi) + \tilde{\omega}_r - \tilde{\Delta} + \tilde{\Delta}/2 - \chi \\
&\approx n(\tilde{\omega}_r - \chi) + (\tilde{\omega}_q - \chi) + \tilde{\Delta}/2, \quad \text{(A3)}
\end{aligned}
$$

where $\chi = g^2/\tilde{\Delta}$ is the dispersive frequency shift. To operate in the so-called nesting regime (i.e., $\omega_{g,0} < \omega_{e,0} < \omega_{e,1} < \omega_{g,1}$) in the driven circuit QED system after the application of the external classical drive field to the transmon qubit, the drive-field frequency must satisfy the nesting condition $\omega_q - 3\chi < \omega_d < \omega_q - \chi$. The drive field applied to the transmon qubit further mixes the dressed states. States $|g,0\rangle$ and $|-,0\rangle \sim |e,0\rangle$ are dressed by the drive field with Rabi frequency Ω_d and the driving frequency ω_d, and we get doubly dressed polariton states

$$
|1\rangle = -\sin\frac{\theta_l}{2}|e,0\rangle + \cos\frac{\theta_l}{2}|g,0\rangle, \quad \text{(A4)}
$$

$$
|2\rangle = \cos\frac{\theta_l}{2}|e,0\rangle + \sin\frac{\theta_l}{2}|g,0\rangle, \quad \text{(A5)}
$$

where $\tan\theta_l = \frac{2\Omega_d}{(\tilde{\omega}_q - \chi)}$. The transition frequency ($\omega_{ij} = \omega_i - \omega_j$) between states $|1\rangle$ and $|2\rangle$ is given by

$$
\omega_{21} = \sqrt{(\tilde{\omega}_q - \chi)^2 + 4\Omega_d^2}. \quad \text{(A6)}
$$

Similarly, The doubly dressed polariton states obtained by mixing states $|+,0\rangle \sim |g,1\rangle$ and $|-,1\rangle \sim |e,1\rangle$ can be expressed as

$$
|3\rangle = -\sin\frac{\theta_u}{2}|g,1\rangle + \cos\frac{\theta_u}{2}|e,1\rangle, \quad \text{(A7)}
$$

$$
|4\rangle = \cos\frac{\theta_u}{2}|g,1\rangle + \sin\frac{\theta_u}{2}|e,1\rangle, \quad \text{(A8)}
$$

where $\tan\theta_u = \frac{2\Omega_d}{(-\tilde{\omega}_q + 3\chi)}$ and the corresponding energy splitting between states $|3\rangle$ and $|4\rangle$ is given by

$$
\omega_{43} = \sqrt{(\tilde{\omega}_q - 3\chi)^2 + 4\Omega_d^2}. \quad \text{(A9)}
$$

APPENDIX B: DERIVATION OF THE COUNTERDIABATIC DRIVE

The expression for the counterdiabatic drive field can be derived by using Eq. (20) as follows:

$$
\begin{aligned}
\Omega_a(t) &= 2\dot{\theta} = 2\left(\frac{\Omega_s(t)\dot{\Omega}_p(t) - \Omega_p(t)\dot{\Omega}_s(t)}{\Omega_p^2(t) + \Omega_s^2(t)}\right) \\
&= \frac{-2t_s/\sigma^2}{2\cosh\left[(t_s^2 - 2tt_s)/2\sigma^2\right]} \\
&= \frac{-t_s}{\sigma^2}\,\text{sech}\left[(t_s^2 - 2tt_s)/2\sigma^2\right], \quad \text{(B1)}
\end{aligned}
$$

where we have used the approximation $\Omega_p = \Omega_s$ (i.e., the Rabi frequencies of the pump and the Stokes fields are equal) for the simplicity of calculation.

[1] M. A. Nielsen and I. L. Chuang, *Quantum Computation and Quantum Information*, 10th anniversary ed. (Cambridge University Press, Cambridge, 2010).

[2] J. Q. You and F. Nori, Nature (London) **474**, 589 (2011).

[3] N. V. Vitanov, A. A. Rangelov, B. W. Shore, and K. Bergmann, Rev. Mod. Phys. **89**, 015006 (2017).

[4] D. Guéry-Odelin, A. Ruschhaupt, A. Kiely, E. Torrontegui, S. Martínez-Garaot, and J. G. Muga, Rev. Mod. Phys. **91**, 045001 (2019).

[5] L. Giannelli and E. Arimondo, Phys. Rev. A **89**, 033419 (2014).

[6] A. Vepsäläinen, S. Danilin, and G. S. Paraoanu, Sci. Adv. **5**, eaau5999 (2019).

[7] X. Gu, A. F. Kockum, A. Miranowicz, Y. X. Liu, and F. Nori, Phys. Rep. **718**, 1 (2017).

[8] A. Blais, A. L. Grimsmo, S. M. Girvin, and A. Wallraff, Rev. Mod. Phys. **93**, 025005 (2021).

[9] S. E. Harris, J. E. Field, and A. Imamoğlu, Phys. Rev. Lett. **64**, 1107 (1990).

[10] S. H. Autler and C. H. Townes, Phys. Rev. **100**, 703 (1955).

[11] G. Alzetta, A. Gozzini, L. Moi, and G. Orriols, Nuovo Cimento B **36**, 5 (1976).

[12] A. A. Abdumalikov, O. Astafiev, A. M. Zagoskin, Y. A. Pashkin, Y. Nakamura, and J. S. Tsai, Phys. Rev. Lett. **104**, 193601 (2010).

[13] S. Novikov, T. Sweeney, J. E. Robinson, S. P. Premaratne, B. Suri, F. C. Wellstood, and B. S. Palmer, Nat. Phys. **12**, 75 (2016).

[14] M. Baur, S. Filipp, R. Bianchetti, J. M. Fink, M. Göppl, L. Steffen, P. J. Leek, A. Blais, and A. Wallraff, Phys. Rev. Lett. **102**, 243602 (2009).

[15] S. Novikov, J. E. Robinson, Z. K. Keane, B. Suri, F. C. Wellstood, and B. S. Palmer, Phys. Rev. B **88**, 060503(R) (2013).

[16] B. Suri, Z. K. Keane, R. Ruskov, L. S. Bishop, C. Tahan, S. Novikov, J. E. Robinson, F. C. Wellstood, and B. S. Palmer, New J. Phys. **15**, 125007 (2013).

[17] W. R. Kelly, Z. Dutton, J. Schlafer, B. Mookerji, T. A. Ohki, J. S. Kline, and D. P. Pappas, Phys. Rev. Lett. **104**, 163601 (2010).

[18] U. Gaubatz, P. Rudecki, M. Becker, S. Schiemann, M. Külz, and K. Bergmann, Chem. Phys. Lett. **149**, 463 (1988).

[19] J. Siewert, T. Brandes, and G. Falci, Opt. Commun. **264**, 435 (2006).

[20] Y. X. Liu, J. Q. You, L. F. Wei, C. P. Sun, and F. Nori, Phys. Rev. Lett. **95**, 087001 (2005).

[21] G. Falci, A. La Cognata, M. Berritta, A. D'Arrigo, E. Paladino, and B. Spagnolo, Phys. Rev. B **87**, 214515 (2013).

[22] P. G. Di Stefano, E. Paladino, A. D'Arrigo, and G. Falci, Phys. Rev. B **91**, 224506 (2015).

[23] P. G. Di Stefano, E. Paladino, T. J. Pope, and G. Falci, Phys. Rev. A **93**, 051801(R) (2016).

[24] W. Zheng, Y. Zhang, Y. Dong, J. Xu, Z. Wang, X. Wang, Y. Li, D. Lan, J. Zhao, S. Li, X. Tan, and Y. Yu, npj Quantum Inf. **8**, 9 (2022).

[25] K. S. Kumar, A. Vepsäläinen, S. Danilin, and G. S. Paraoanu, Nat. Commun. **7**, 10628 (2016).

[26] H. K. Xu, C. Song, W. Y. Liu, G. M. Xue, F. F. Su, H. Deng, Y. Tian, D. N. Zheng, S. Han, Y. P. Zhong, H. Wang, Y. X. Liu, and S. P. Zhao, Nat. Commun. **7**, 11018 (2016).

[27] X. Chen, A. Ruschhaupt, S. Schmidt, A. del Campo, D. Guéry-Odelin, and J. G. Muga, Phys. Rev. Lett. **104**, 063002 (2010).

[28] M. V. Berry, J. Phys. A **42**, 365303 (2009).

[29] X. Chen, E. Torrontegui, and J. G. Muga, Phys. Rev. A **83**, 062116 (2011).

[30] X. Chen and J. G. Muga, Phys. Rev. A **86**, 033405 (2012).

[31] A. Baksic, H. Ribeiro, and A. A. Clerk, Phys. Rev. Lett. **116**, 230503 (2016).

[32] Y.-C. Li and X. Chen, Phys. Rev. A **94**, 063411 (2016).

[33] K. Koshino, K. Inomata, T. Yamamoto, and Y. Nakamura, Phys. Rev. Lett. **111**, 153601 (2013).

[34] K. Inomata, K. Koshino, Z. R. Lin, W. D. Oliver, J. S. Tsai, Y. Nakamura, and T. Yamamoto, Phys. Rev. Lett. **113**, 063604 (2014).

[35] K. Inomata, Z. Lin, K. Koshino, W. D. Oliver, J.-S. Tsai, T. Yamamoto, and Y. Nakamura, Nat. Commun. **7**, 12303 (2016).

[36] K. Koshino, K. Inomata, Z. R. Lin, Y. Tokunaga, T. Yamamoto, and Y. Nakamura, Phys. Rev. Appl. **7**, 064006 (2017).

[37] X. Gu, S.-N. Huai, F. Nori, and Y. X. Liu, Phys. Rev. A **93**, 063827 (2016).

[38] J. Long, H. S. Ku, X. Wu, X. Gu, R. E. Lake, M. Bal, Y. X. Liu, and D. P. Pappas, Phys. Rev. Lett. **120**, 083602 (2018).

[39] G. Ithier, E. Collin, P. Joyez, P. J. Meeson, D. Vion, D. Esteve, F. Chiarello, A. Shnirman, Y. Makhlin, J. Schriefl, and G. Schön, Phys. Rev. B **72**, 134519 (2005).

[40] L. S. Theis, F. Motzoi, S. Machnes, and F. K. Wilhelm, Europhys. Lett. **123**, 60001 (2018).

[41] J. R. Kuklinski, U. Gaubatz, F. T. Hioe, and K. Bergmann, Phys. Rev. A **40**, 6741 (1989).

[42] X. Chen, I. Lizuain, A. Ruschhaupt, D. Guéry-Odelin, and J. G. Muga, Phys. Rev. Lett. **105**, 123003 (2010).

[43] C. W. Gardinerand and P. Zoller, *Quantum Noise a Handbook of Markovian and Non-Markovian Quantum Stochastic Methods with Applications to Quantum Optics*, Springer Series in Synergetics, 3rd ed. (Springer, Berlin, Heidelberg, 2004).

[44] A. A. Clerk, M. H. Devoret, S. M. Girvin, F. Marquardt, and R. J. Schoelkopf, Rev. Mod. Phys. **82**, 1155 (2010).

[45] J. Johansson, P. Nation, and F. Nori, Comput. Phys. Commun. **183**, 1760 (2012).

[46] J. Johansson, P. Nation, and F. Nori, Comput. Phys. Commun. **184**, 1234 (2013).

[47] K. Bergmann, N. V. Vitanov, and B. W. Shore, J. Chem. Phys. **142**, 170901 (2015).

[48] N. V. Vitanov, K.-A. Suominen, and B. W. Shore, J. Phys. B **32**, 4535 (1999).

[49] F. Petiziol, E. Arimondo, L. Giannelli, F. Mintert, and S. Wimberger, Sci. Rep. **10**, 2185 (2020).

[50] Y.-H. Chen, W. Qin, X. Wang, A. Miranowicz, and F. Nori, Phys. Rev. Lett. **126**, 023602 (2021).

[51] D. Møller, L. B. Madsen, and K. Mølmer, Phys. Rev. A **77**, 022306 (2008).

[52] T. Yan, B.-J. Liu, K. Xu, C. Song, S. Liu, Z. Zhang, H. Deng, Z. Yan, H. Rong, K. Huang, M.-H. Yung, Y. Chen, and D. Yu, Phys. Rev. Lett. **122**, 080501 (2019).